Superlattices and Microstructures 88 (2015) 480–488

Contents lists available at ScienceDirect

Superlattices and Microstructures

journal homepage: www.elsevier.com/locate/superlattices

Growth of non-polar InGaN quantum dots with an underlying AlN/GaN distributed Bragg reflector by metal-organic vapour phase epitaxy

Tongtong Zhu [a, *], James T. Griffiths [a], Wai Yuen Fu [a], Ashley Howkins [b], Ian W. Boyd [b], Menno J. Kappers [a], Rachel A. Oliver [a]

[a] Department of Materials Science and Metallurgy, University of Cambridge, 27 Charles Babbage Road, Cambridge CB3 0FS, United Kingdom
[b] Experimental Techniques Centre, Brunel University, Uxbridge UB8 3PH, United Kingdom

ARTICLE INFO

Article history:
Received 7 July 2015
Received in revised form 29 September 2015
Accepted 1 October 2015
Available online 9 October 2015

Keywords:
Cathodoluminescence
Nitride
InGaN quantum dots
Metal-organic vapour phase epitaxy

ABSTRACT

Non-polar (11–20) InGaN quantum dots (QDs) have been grown using a modified droplet epitaxy method by metal-organic vapour phase epitaxy on top of a 15-period AlN/GaN distributed Bragg reflector (DBR) on *a*-plane GaN pseudo-substrate prepared by epitaxial lateral overgrowth (ELOG), in which the QDs are located at the centre of a ca. 180 nm GaN layer. The AlN/GaN DBR has shown a peak reflectivity of ~80% at a wavelength of ~454 nm with a 49 nm wide, flat stop-band. Variations in layer thicknesses observed by cross-sectional scanning transmission electron microscopy have been identified as the main source of degradation of the DBR reflectivity. The presence of trenches due to incomplete coalescence of the ELOG template and the formation of cracks due to relaxation of tensile strain during the DBR growth may distort the DBR and further reduce the reflectivity. The DBR top surface is very smooth and does not have a detrimental effect on the subsequent growth of QDs. Enhanced single QD emission at 20 K was observed in cathodoluminescence.

1. Introduction

Nitride quantum dots (QDs) offer great potential to achieve single photon emission at room temperature [1], due to the large band offset between the quantum dot structure and the matrix and the large exciton binding energy [2]. However, quantum dot structures grown on the polar (0001) plane contain significant inherent spontaneous and piezoelectric polarisations directed along the [0001] axis. The resulting electric fields lead to spatial separation of the electron and hole wavefunctions, which reduces the radiative recombination efficiency, leads to long exciton lifetimes, and may also be partly responsible for the variation in the emission wavelength and linewidth over time [3,4]. However, growth of non-polar InGaN QDs with much shorter exciton recombination lifetimes [5] (an order of magnitude lower than the corresponding polar equivalent structures [6]) has recently been demonstrated. Such non-polar InGaN QDs also exhibit improved temperature

* Corresponding author.
E-mail address: tz234@cam.ac.uk (T. Zhu).

http://dx.doi.org/10.1016/j.spmi.2015.10.001

stability: no significant linewidth broadening was observed up to 120 K [7]. Furthermore, the first Rabi oscillations in the InGaN QD system have also been observed in these non-polar structures [8].

High quality nitride microcavity structures can provide new insights into light-matter interactions and fundamental physics [9–11]. A distributed Bragg reflector (DBR) is an efficient reflective buffer structure, which has been widely used for GaN-based microcavities, and may be grown *in-situ* during the same run as the QD structures [12–15]. With the superior optical properties of non-polar InGaN QDs, high quality, high reflectivity DBRs are needed to enhance the spontaneous emission rate and light extraction efficiency for single photon source applications [15], and are also relevant to more conventional non-polar GaN-based opto-electronic devices, such as resonant cavity light emitting diodes (RCLEDs) [16] and vertical cavity surface emitting lasers (VCSELs) [17,18].

In this paper, we report on the growth of a 15-period AlN/GaN DBR on *a*-plane GaN template, prepared by epitaxial lateral overgrowth (ELOG) by metal-organic vapour phase epitxay (MOVPE). QD structures are then grown within a GaN layer on top of this DBR. We have observed enhanced QD emission based on this structure in CL at 20 K, suggesting the light extraction efficiency of single QD emission has been increased. This marks an important step towards the development of devices based on non-polar InGaN QDs in microcavities.

2. Experimental details

All non-polar *a*-plane (11–20) samples were grown on *r*-plane sapphire by MOVPE in a Thomas Swan close-coupled showerhead reactor using tri-methyl indium (TMI), tri-methyl gallium (TMG), tri-methyl aluminium (TMA) and ammonia as precursors. To prepare *a*-plane GaN templates with low defect densities and a smooth surface morphology, we have used the ELOG method. After the growth of a 1 μm GaN buffer layer with a V/III ratio of 60 at 1050 °C following a 30 nm GaN nucleation layer grown at 540 °C and 500 Torr, a 100 nm thick SiO_2 layer was deposited and patterned into 6 μm wide stripes and 4 μm window openings along the [1–100] direction using conventional wet chemistry photolithography. Regrowth was carried out in a single step using a V/III ratio of 60 at 1050 °C and 100 Torr to enhance lateral growth and coalescence, which was followed by an additional 2 μm of GaN growth at a higher V/III ratio of 740 to improve the optical properties [19].

In order to assess the development of the microstructure during growth and the impact of the bottom DBR on the subsequent layer growth, a few test samples have also been grown and are shown schematically in Fig. 1. A 15-period AlN/GaN DBR stack was designed to provide a peak reflectivity of ~96% at 451 nm based on a model using a transfer matrix method [20]. The nominal thickness (λ/4) for each GaN and AlN layer was 47.1 nm and 53.1 nm, respectively. Another 90 nm GaN layer was subsequently grown on top of the DBR stack (sample A), followed by an InGaN QD layer (sample B), which was grown via

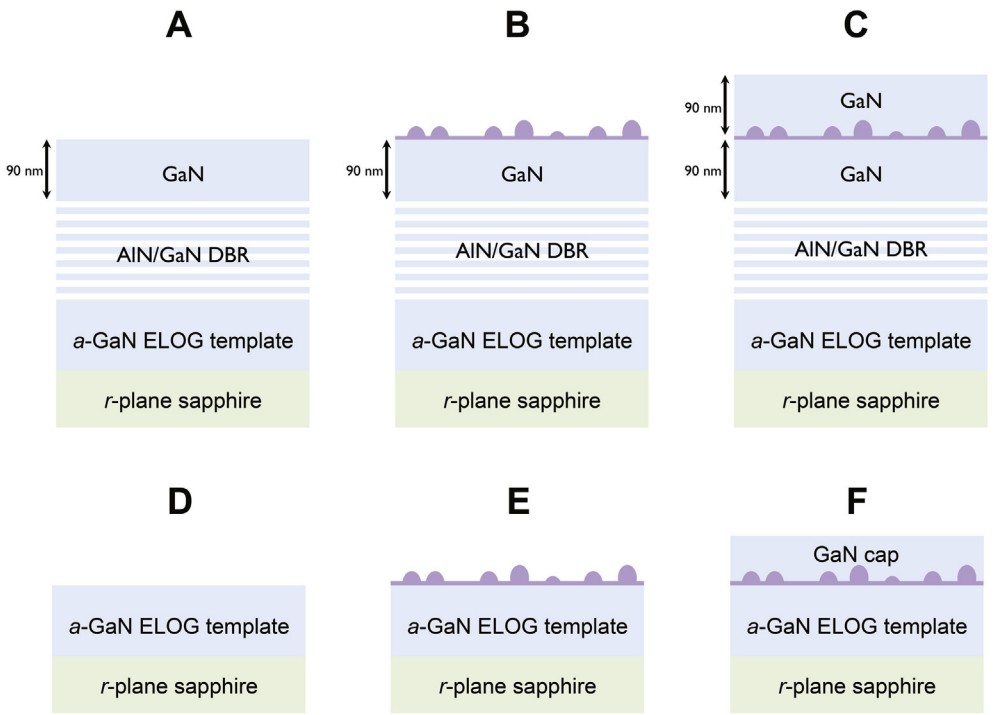

Fig. 1. Schematic diagram of the structures of sample A – F. Sample A – AlN/GaN DBR and a 90 nm GaN; Sample B – uncapped InGaN QD layer on DBR +90 nm GaN; Sample C – InGaN QDs at the centre of 180 nm GaN layer on top of DBR; Sample D – *a*-plane ELOG template on *r*-plane sapphire; Sample E – uncapped InGaN QD directly grown on top of ELOG; Sample F – capped InGaN QDs on ELOG template.

a modified droplet epitaxy method. Details of our QD growth can be found elsewhere [5]. Finally, the InGaN QDs were capped by another 90 nm of GaN (sample C) to complete the full structure, and a cavity would be formed if a top DBR was added. We compare the surface morphologies of these samples to similar structures grown directly on GaN ELOG pseudo-substrates with no DBR (sample D – F).

Surface morphologies were examined using a Veeco Dimension 3100 atomic force microscope (AFM) with a Nanoscope V controller in TappingMode™. RTESP tips from Bruker-Nano with a nominal end radius of 8 nm were employed. The DBR microstructure was characterized in cross-section by scanning transmission electron microscopy (STEM) at 200 keV. Bright field STEM (BF-STEM) imaging was performed on a JEOL 2100F Schottky field emission gun (FEG) TEM. High angle annular dark field (HAADF-STEM) was performed on a FEI Technai Osiris X-FEG TEM. STEM samples were prepared by mechanical polishing, followed by Ar^+ ion milling at 5 keV and subsequent low energy ion milling at 0.5 keV to minimise specimen damage. Room temperature DBR reflectivity was measured by an Accent RPM2000 photoluminescence and reflectivity mapper with a typical spot size of 1 mm^2, and normalized with a calibrated silver mirror using the same measurement parameters. CL measurements were carried out on a liquid helium cooled stage at 20 K in a Philips XL30s scanning electron microscope operating at 8 kV and equipped with a Gatan MonoCL4 system.

3. Results and discussion

3.1. Microstructural characterization of DBR samples

Fig. 2(a) shows a typical surface of the *a*-plane GaN ELOG pseudo-substrate (sample D). The surface morphology of the highly defective window is dominated by surface pits associated with dislocations and appears much rougher than the low defect density wing. The root-mean-square (rms) roughness of the *a*-plane ELOG pseudo-substrate over a 10 μm × 10 μm area is 2.9 nm [Fig. 2(a)] and over a 4 μm × 4 μm area in the wing region it is 0.6 nm [Fig. 2(b)]. Previous studies of *a*-plane ELOG GaN samples [21] suggest that the window regions typically have a dislocation density is 1 × 10^{10} cm^{-2} and a basal plane stacking fault (BSF) density of 1 × 10^6 cm^{-1}, while the wing regions have a dislocation density of 9 × 10^8 cm^{-2} and a BSF density of 2 × 10^4 cm^{-1}. The linear features seen in Fig. 2(b) could be BSF related. To assess the impact of a bottom AlN/GaN

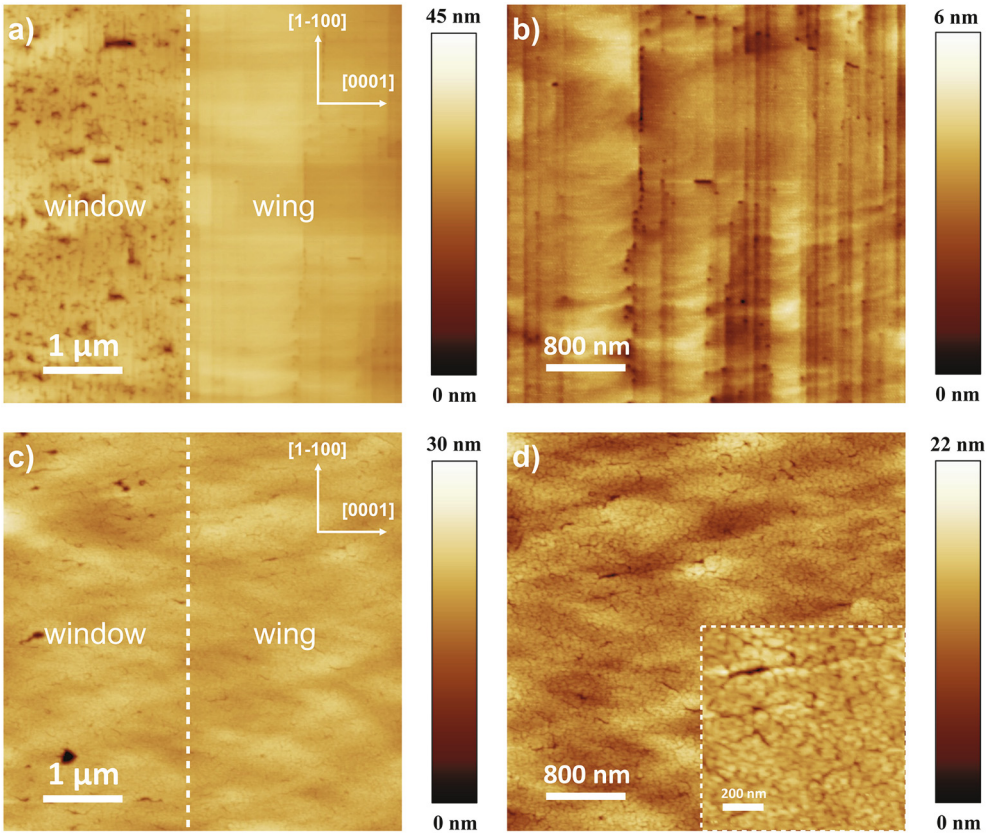

Fig. 2. AFM images of a) Sample D – *a*-plane GaN ELOG template, c) Sample A – a 15-period AlN/GaN DBR on *a*-plane GaN ELOG with a 90 nm GaN layer. Zoomed in images taken from the low-defect density wing regions b) and d), Inset: 1 × 1 μm^2 scan from the wing.

DBR on any subsequent growth of InGaN QDs, a 15-period AlN/GaN DBR stack with a 90 nm GaN layer was firstly grown (sample A). The overall rms roughness over a 10 μm × 10 μm area is 2.9 nm, which is identical to sample D within the experimental errors. However, the top surface of the DBR sample (sample A) exhibits a network of fissures as opposed to a terraced morphology in the wing region of sample D, so that at a smaller scale, the surface is somewhat rougher than that of the ELOG pseudo-substrate [Fig. 2(c)], with an rms roughness of about 1.7 nm over a 4 μm × 4 μm scan [Fig. 2(d)]. However, this roughness remains low in absolute terms and unlikely to be prohibitive for subsequent QD growth. A summary of rms roughness for different samples is given in Table 1.

The uncapped QD layer grown directly on the ELOG template (sample E) shows large surface holes and the associated large indium/gallium metallic droplets in Fig. 3(a). Although, the observation of both holes and large droplets is still under investigation, the general surface morphology and the presence of an underlying network structure of interconnected InGaN strips [indicated by the white arrows in the inset of Fig. 3(b)] appear to be similar to what we have reported earlier [5,22].

The uncapped QD layer grown on top of the DBR +90 nm GaN (sample B), showed a similar surface morphology to sample A as seen in Fig. 2(c). Nanostructures can also be seen on the surface in both window and wing regions. It appears that the nanostructures in this case are much smaller (average height ~21 nm), but with a similar density (~1.5×10^8 cm^{-2}) as compared to the control sample E (for which the average height is ~44 nm and the density is ~1.4×10^8 cm^{-2}). However, it should be noted that these values vary across the sample surface for both samples (For sample B, the maximum density is ~2.7×10^8 cm^{-2}, and minimum density is ~7×10^7 cm^{-2}), and the differences between samples and within specific samples may be more linked to variations in the InGaN growth temperature than to the underlying DBR structure. The density and average height of the nanostructures for the uncapped QD samples are summarized in Table 2.

For the capped samples, the sample grown directly on a GaN ELOG pseudo-substrate (sample F) exhibits a pitted window and a smooth wing surface in Fig. 3(c and d). On the other hand, Fig. 3(g and h) show that the capped sample grown on the AlN/GaN DBR (sample C) exhibits a similar surface morphology to the DBR sample without QDs (sample A) [Fig. 2(c and d)], with a similar network of fissures over the wing region. The rms roughness of the wing region for the DBR sample C is 1.65 nm over a 4 μm × 4 μm scan area, whereas for the control sample F is 0.39 nm. Again, whilst the underlying DBR does introduce roughness, it is not of a magnitude which would be prohibitive for the growth of a further reflector on top of the GaN cap. It is worth noting that differential interference contrast optical microscopy shows that there are no cracks on the ELOG template (sample D) [Fig. 4(a)], but that some uncoalesced trenches along the [1–100] direction may be observed. After the growth of the full structure (sample C), the surface exhibits cracks that run predominantly along [0001] [Fig. 4(b)].

Further insight into the microstructure of the DBR sample was obtained by cross-sectional STEM analysis. Fig. 5(a) shows an overview of sample C (which includes a DBR and a capped QD layer) in which the highly defective window and low defect density wing regions of the ELOG pseudo-substrate can be clearly seen, as well as the DBR stack towards the top surface of the sample. We observe trenches running along the [1–100] direction parallel to the ELOG mask orientation. These trenches are visible before the growth of the DBR stack as shown in Fig. 5(b) and relate to incomplete coalescence of the ELOG stripes. They become larger and wider as the DBR growth proceeds. Just prior to where the growth of the DBR started, the two sides of the trench were not quite level. (The offset is ~70 nm). However, by the time the last layer of the DBR was grown, this discrepancy had been reduced, implying local inhomogeneity of the layer thickness of the DBR layers on the *a*-plane. In fact, the measured average thicknesses of GaN on either side of the trench seem to be fairly consistent (47.5 ± 0.5 nm in the wing, whereas 48.4 ± 0.7 nm in the window). But the average AlN thickness in the wing (53.3 ± 0.6 nm) is thicker than that in the window (48.8 ± 0.8 nm).

The AlN layers relating to the DBR continue into the trench but are thinner on the side facets of the trench than on the *a*-plane surface, in which the vertical facet is (0001) and the ~60° inclined facet is therefore expected to be (11-2-2). The GaN and AlN layer thicknesses along the inclined (11-2-2) facet have been measured to be 20 ± 5.5 nm and 22.5 ± 5 nm, respectively, suggesting that the overall growth rate for the (11–22) DBR stack is slower than for the *a*-plane growth. However, the multilayer structure cannot be clearly resolved for the growth along the *c*-axis. Nevertheless, most of the AlN/GaN interfaces are very well defined and uniform across the highly defective window and the low defect density wing regions [Fig. 5(c)]. The QD layer can also be seen located in the centre of the 180 nm GaN layer [Fig. 5(d)]. Further microscopy studies are underway to obtain more microstructural details of the InGaN QD layer.

A closer look at the interface between the first AlN layer to be grown and the underlying GaN in Fig. 5(e) reveals voids along [1–100] with a spacing ~120 nm, which are absent if the DBR is viewed along [0001] as shown in Fig. 5(f). This suggests that the strain in the [0001] direction relaxed fully or partially during the growth of the first AlN layer by the formation of small cracks which then healed via lateral overgrowth to reduce the surface energy. Similar features have been observed by Zhu *et al.* [23] in their studies of *a*-plane AlN/GaN DBRs, and have been attributed to plastic relaxation of tensile strain. These

Table 1
Summary of RMS roughness for different samples (A, C, D, and F).

Samples	RMS roughness (nm) (10 μm × 10 μm)	RMS roughness (nm) (4 μm × 4 μm)
A (DBR an ELOG)	2.9	1.7
C (capped QDs on DBR)	3.3	1.65
D (ELOG pseudo-substrate)	2.9	0.6
F (capped QDs on ELOG)	1.77	0.39

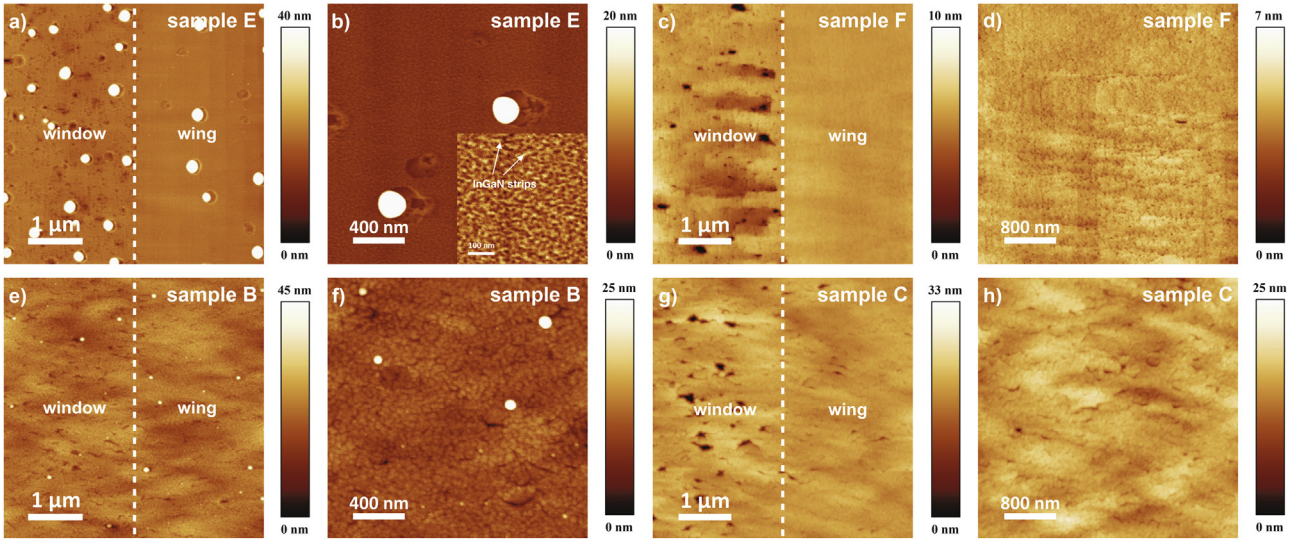

Fig. 3. AFM images of a) sample E and e) sample B – uncapped InGaN QD layer, and c) sample F and g) sample C – capped InGaN QDs with a GaN cap grown on top of GaN ELOG pseudo-substrates on top of an AlN/GaN DBR, respectively. b), d), f), and h) are zoomed in images taken from the low-defect density wing regions of a), c), e) and g) respectively.

Table 2
Summary of the density and average height of the nanostructures for the uncapped QD samples (B and E).

Samples	Density (cm^{-2})	Average height (nm)
B (uncapped QDs on DBR)	1.5×10^8	21
E (uncapped QDs on ELOG)	1.4×10^8	44

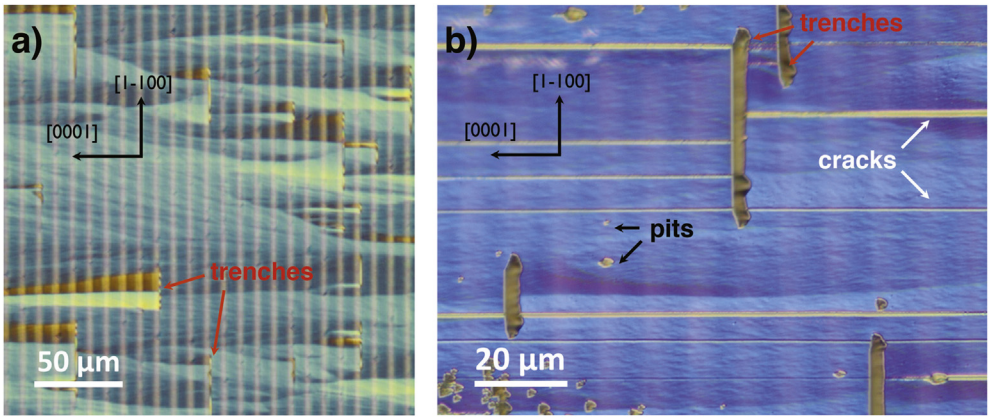

Fig. 4. Surface morphology of a) Sample D and b) Sample C by Nomarski interference light microscopy, showing trenches (uncoalesced regions during ELOG growth, indicated by the red arrows), cracks (marked as white arrows), and dislocation related surface pits (black arrows). (For interpretation of the references to colour in this figure legend, the reader is referred to the web version of this article.)

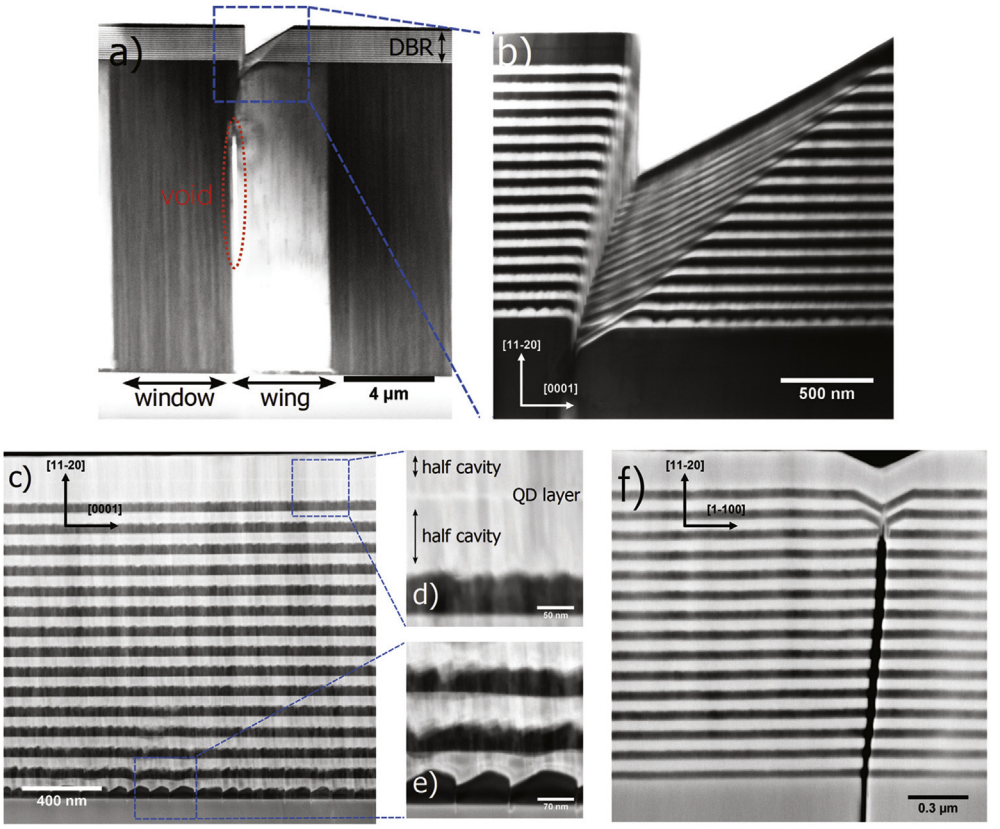

Fig. 5. Cross-sectional STEM images of sample C - the capped QD sample grown on top of a 15-period AlN/GaN DBR. a,b) BF-STEM images; c,d,e) HAADF images viewed along [1–100], whilst f) is viewed along [0001].

features lead to relaxation along the [0001] direction but higher tensile strain will be accumulated along the [1–100] direction during the DBR growth, and this is likely to be the origin of the observed macroscopic cracks perpendicular to the [1–100]. One of the macroscopic cracks along the [0001] direction has also been imaged by STEM and is shown in Fig. 5(f). The fact that the first 12 layers appear undistorted by the crack may suggest that this crack did not form until ca. 13 layers had been grown. Assuming the crack formed around layer 13, it then propagated through the DBR stack reliving strain and may also have propagated into the ELOG GaN template as seen in Fig. 5(f). Alternatively, the observed feature in the ELOG template may have resulted from the TEM sample preparation. During growth of the last two layers, in which the DBR is distorted, the crack appears to have been healed up.

Throughout the stack, the top surfaces of the AlN layers are rougher than those of the GaN layers. And it is worth noting that the surface of the first AlN layer is much rougher than that of subsequent layers. This suggests that the formation of the buried cracks in the first AlN layer is also associated with roughening of the layer, whereas the subsequent, more relaxed layers grow with a smoother morphology. The roughening itself may also provide some strain relief during growth, similar to the fissure structure observed in the growth of AlN on GaN on the *c*-plane [15].

3.2. Reflectivity characterization of DBR samples

The reflectivity measurement of the DBR sample A was performed at room temperature and shown in Fig. 6, and was compared with model reflectivity data for the original intended structure (blue curve) calculated using a transfer matrix method (47.1 nm thick GaN and 53.1 nm thick for AlN). For the real DBR sample, the reflectivity (black curve) is around 80 ± 2% across the window and wing regions (spot size ~1 mm^2). The stop-band position is ~454 nm and the width of the stop-band is ~49 nm. Although by using the average layer thicknesses in the wing obtained from the STEM analysis, we are able to reproduce the experimental stop-band position and width in the transfer matrix model (red curve), the stop-band is observed to be blue-shifted to ~439 nm if the thickness values measured from the window are used (cyan curve).

However, the measured reflectivity is less than the predicted value (~96%), which is likely to relate to, amongst other factors, the roughness of the GaN/AlN interfaces particularly for the first layer in the DBR stack and the non-uniformity of the DBR layer thicknesses. Using STEM measurements of the thickness of each layer (on the *a*-plane) through the thickness of the stack, we calculate a new model (green curve) in which the overall reflectivity is reduced to 85%. This implies that variations in layer thickness through the stack are the main source of the reduced reflectivity in comparison to the model. In fact, a closer look at the cross-sectional STEM data and a careful extraction of layer thickness have revealed that whilst the layer thicknesses are fairly consistent through the DBR stack in the wing regions, there is a monotonic variation in the measured layer thicknesses in the window regions. (The GaN layer width smoothly increases, while the AlN layer thickness decreases through the DBR stack.). This observation could potentially be of practical importance, for samples grown on templates with a uniform defect density, as one could achieve much better reflectivities simply by altering the growth time to counteract the change in growth rate. This possibility is the subject of ongoing investigations. In addition, the presence of cracks and trenches in the top surface may also reduce the measured reflectivity further.

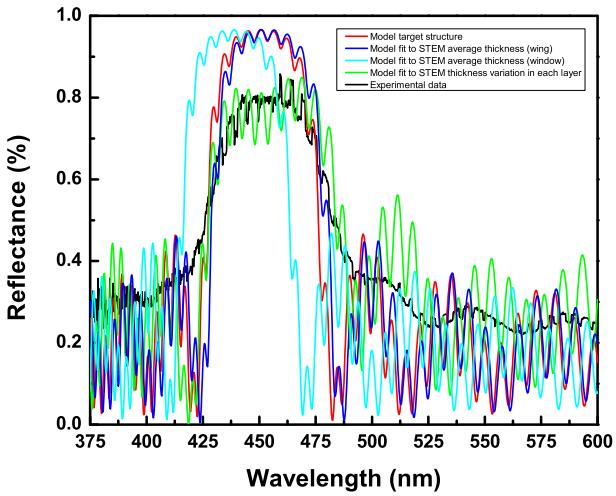

Fig. 6. Reflectivity of Sample A – a 15-period AlN/GaN DBR + 90 nm GaN. The blue curve is the reflectivity of the intended structure. The red curve shows the calculated reflectivity based on the average layer thicknesses in the wing measured by STEM (GaN is 47.5 nm and AlN is 53.3 nm). The cyan curve shows the calculated reflectivity based on the average layer thicknesses in the window measured by STEM (GaN is 48.4 nm and AlN is 48.8 nm). The black curve is the measured reflectivity. The green curve is the calculated reflectivity including thickness variation in each layer through the DBR stack as measured by STEM. (For interpretation of the references to colour in this figure legend, the reader is referred to the web version of this article.)

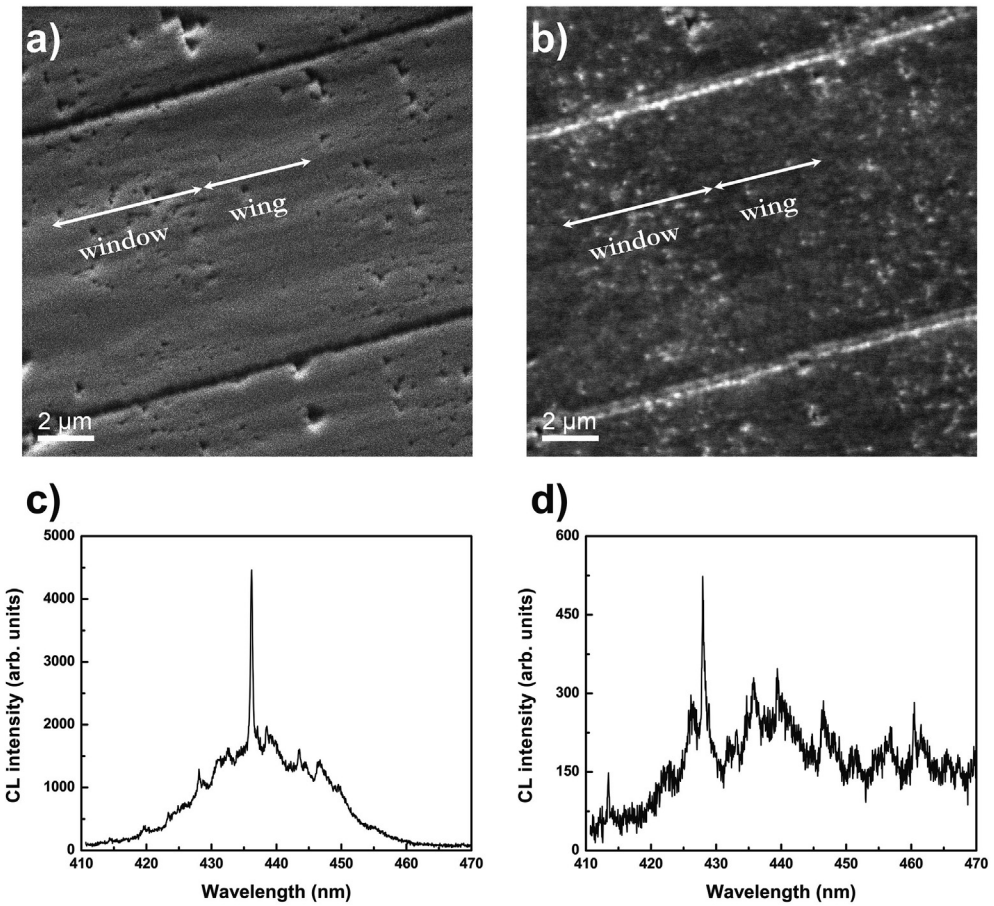

Fig. 7. a) SEM and b) panchromatic CL images of the capped QD sample with a 15-period AlN/GaN DBR (sample C). Typical CL spectra taken at 20 K from samples c) with DBR (sample C) and d) without a DBR (sample F) on ELOG pseudo-substrates.

3.3. Cathodoluminescence characterization of the QD sample

To investigate the optical properties of the subsequent QD growth on top of the DBR, CL has been performed at 20 K. Fig. 7(a and b) show the SEM and panchromatic CL images (all the photons collected are detected by the photomultiplier tube with no wavelength selection) of the QD on DBR sample. Bright spots are observed, but it is worth noting that the bright spots in the window regions and the cracks appear to be brighter than that in the wing regions. This might be due to the presence of faceted surface pits/cracks and thus different light extraction in these regions.

Fig. 7(c) shows a typical CL spectrum taken at 20 K from sample C, a strong sharp peak, related to emission from a single QD is observed at ~436 nm (which have previously been identified as InGaN QD excitons [7,8]), in the spectral range corresponding to the stop-band of the DBR. The measured linewidths of the QD peaks are typically ~2 meV, which are limited by the spectral resolution of the CL setup and consistent with our earlier findings [5,22]. Moreover, the QD emission in this sample exhibits up to 10 times more intensity than that from a QD sample grown directly on ELOG pseudo-substrate without a DBR (sample F) under the same CL excitation conditions at 20 K [Fig. 7(d)]. We attribute this enhancement not only to the fact that the lower DBR and the top surface together do form a low quality factor cavity, but also it is possible that the QD structure and properties (i.e. internal quantum efficiency) may have been altered to some extent by the underlying DBR. Additionally, the presence of AlN layers may prevent carrier diffusion away from the QD layer to some extent leading to enhanced carrier injection efficiency.

4. Conclusion

In summary, we have demonstrated the growth and characterization of a 15-period AlN/GaN DBR on ELOG template, which has a peak reflectivity of ~80% at 454 nm. The factors that degrade the reflectivity have been identified and discussed, and attributed mainly to the variations in layer thicknesses through the DBR stack. Incorporation of non-polar (11−20) InGaN QDs at the centre of a 180 nm thick GaN layer on top of the DBR has been carried out via modified droplet epitaxy. Enhanced

emission from single InGaN QDs has been observed in CL at 20 K. Incorporation of non-polar (11–20) InGaN QDs with an underlying AlN/GaN DBR demonstrates great potential for single photon source device development in the future.

Acknowledgements

The authors acknowledge Dr. Alexander Woolf, for assistance with the ELOG sample growth. This work has been funded by the EPSRC (Grant No. EP/H047816/1 and EP/J001627/1).

Appendix A. Supporting information

Datasets for the figures in this paper can be found at https://www.repository.cam.ac.uk/handle/1810/251381.

References

[1] M.J. Holmes, K. Choi, S. Kako, M. Arita, Y. Arakawa, Nano Lett. 14 (2014) 982.
[2] S. Kako, C. Santori, K. Hoshino, S. Götzinger, Y. Yamamoto, Y. Arakawa, Nat. Mater. 5 (2006) 887.
[3] J.H. Rice, J.W. Robinson, A. Jarjour, R.A. Taylor, R.A. Oliver, G.A.D. Briggs, M.J. Kappers, C.J. Humphreys, Appl. Phys. Lett. 84 (2004) 4110.
[4] S. Schulz, E.P. O'Reilly, Appl. Phys. Lett. 99 (2011) 223106.
[5] T. Zhu, F. Oehler, B.P.L. Reid, R.M. Emery, R.A. Taylor, M.J. Kappers, R.A. Oliver, Appl. Phys. Lett. 102 (2013) 251905.
[6] R.A. Oliver, G.A.D. Briggs, M.J. Kappers, C.J. Humphreys, S. Yasin, J.H. Rice, J.D. Smith, R.A. Taylor, Appl. Phys. Lett. 83 (2003) 755.
[7] B.P.L. Reid, T. Zhu, C.C.S. Chan, C. Kocher, F. Oehler, R. Emery, M.J. Kappers, R.A. Oliver, R.A. Taylor, Phys. Status Solidi C 11 (2014) 702.
[8] B.P.L. Reid, C. Kocher, T. Zhu, F. Oehler, R. Emery, C.C.S. Chan, R.A. Oliver, R.A. Taylor, Appl. Phys. Lett. 104 (2014) 263108.
[9] I. Aharonovich, A. Woolf, K.J. Russell, T. Zhu, N. Niu, M.J. Kappers, R.A. Oliver, E.L. Hu, Appl. Phys. Lett. 103 (2013) 021112.
[10] N.V. Triviño, R. Butté, J. Carlin, N. Grandjean, Nano Lett. 15 (2015) 1259.
[11] A. Woolf, T. Puchtler, I. Aharanovich, T. Zhu, R.A. Oliver, E.L. Hu, Proc. Natl. Acad. Sci. 111 (2014) 14042.
[12] C. Kruse, H. Dartsch, T. Aschenbrenner, S. Figge, D. Hommel, Phys. Status Solidi B 248 (2011) 1748.
[13] R. Tao, M. Arita, S. Kako, K. Kamide, Y. Arakawa, Appl. Phys. Lett. 107 (2015) 101102.
[14] G. Christmann, R. Butté, E. Feltin, A. Mouti, P.A. Stadelmann, A. Castiglia, J. Carlin, N. Grandjean, Phys. Rev. B 77 (2008) 085310.
[15] R.A. Oliver, A.F. Jarjour, R.A. Taylor, A. Tahraoui, Y. Zhang, M.J. Kappers, C.J. Humphreys, Mater. Sci. Eng. B 147 (2008) 108.
[16] M. Diagne, Y. He, H. Zhou, E. Makarona, A.V. Nurmikko, J. Han, K.E. Waldrip, J.J. Figiel, T. Takeuchi, M. Krames, Appl. Phys. Lett. 79 (2001) 3720.
[17] T. Someya, R. Werner, A. Forchel, M. Catalano, R. Cingolani, Y. Arakawa, Science 285 (1999) 1905.
[18] C. Holder, J.S. Speck, S.P. DenBaars, S. Nakamura, D. Feezell, Appl. Phys. Express 5 (2012) 092104.
[19] M. Häberlen, T.J. Badcock, M.A. Moram, J.L. Hollander, M.J. Kappers, P. Dawson, C.J. Humphreys, R.A. Oliver, J. Appl. Phys. 108 (2010) 033523.
[20] E. Hecht, Optics, third ed., Addison-Wesley Longman, 1998.
[21] C.F. Johnston, M.J. Kappers, M.A. Moram, J.L. Hollander, C.J. Humphreys, Phys. Status Solidi A 206 (2009) 1190.
[22] R.M. Emery, T. Zhu, F. Oehler, B. Reid, R.A. Taylor, M.J. Kappers, R.A. Oliver, Phys. Status Solidi C 11 (2014) 698.
[23] T. Zhu, A. Dussaigne, G. Christmann, C. Pinquier, E. Feltin, D. Martin, R. Butté, N. Grandjean, Appl. Phys. Lett. 92 (2008) 061114.